Journal of Nuclear Materials 447 (2014) 82–93

Contents lists available at ScienceDirect

Journal of Nuclear Materials

journal homepage: www.elsevier.com/locate/jnucmat

Effect of crystallite orientation and external stress on hydride precipitation and dissolution in Zr2.5%Nb

P. Vizcaíno [a], J.R. Santisteban [b,*], M.A. Vicente Alvarez [b], A.D. Banchik [a], J. Almer [c]

[a] Centro Atómico Ezeiza, CNEA, Buenos Aires, Argentina
[b] Centro Atómico Bariloche, CNEA-CONICET e Instituto Balseiro, Bariloche, Argentina
[c] Advanced Photon Source, Argonne National Laboratory, Argonne, IL, USA

ARTICLE INFO

Article history:
Received 20 May 2013
Accepted 24 December 2013
Available online 2 January 2014

ABSTRACT

Thermal cycling of Zr2.5%Nb pressure tubes specimens containing ~100 wt ppm H between room temperature and 400 °C produces the dissolution and re-precipitation of zirconium hydride, with a distinctive hysteresis between these two processes. In this work, we have found that the details of the precipitation and dissolution depend on the actual orientation of the α-Zr grains where hydride precipitation takes place. In situ synchrotron X-ray diffraction experiments during such thermal cycles have provided information about hydride precipitation specific to the two most important groups of α-Zr phase orientations, namely crystallites having *c*-axes parallel (m_{Hoop}) and tilted by ~20° (m_{Tilted}) from the tube hoop direction. The results indicate that hydrides precipitate at slightly higher temperatures (~5 °C), and dissolve at consistently higher temperatures (~15 °C) in m_{Tilted} grains than in m_{Hoop} grains. Moreover, application of a tensile stress along the tube hoop direction results in two noticeable effects in hydride precipitation. Firstly, it shifts hydride precipitation towards higher temperatures, at a rate of ~(0.08 ± 0.02) °C/MPa for hydrides precipitated in the m_{Hoop} grains. Secondly, it produces a redistribution of hydrogen between grains of different orientations, increasing hydride precipitation on those α-Zr grains having their *c*-axes stretched by the external load. A detailed analysis of the diffracted signal shows that such redistribution occurs during the precipitation stage, as a result of changes in the precipitation temperatures for different grain orientations.

© 2013 Elsevier B.V. All rights reserved.

1. Introduction

Metals of the Group IV (Ti, Zr, Hf) dissolve relatively large amounts of interstitial hydrogen (H) at high temperatures. The interstitial H expands the hexagonal crystal lattices increasing the volume of the matrix typically in the order of $\Delta V \sim 2.9$ Å^3 per H atom [1]. Such expansion is slightly anisotropic, hence it is described by a *dilatational* strain tensor e^H_{ij}. Upon cooling to room temperature, some of the hydrogen precipitates as hydrides, and the interstitial H is segregated heterogeneously into a hydride phase, which has a density of the order of 10–20% lower than that of the unhydrided metal phase [2,3]. The crystal structure and morphology of the hydride phase depends on cooling rate, H concentration, stress state and microstructure of the original material. The hydride precipitates are coherent or semi-coherent with the matrix, and result after an additional distortion of the metal lattice (already expanded by the dissolved H). As a result of the large difference in density between hydride and metal, some plastic work is necessary to accommodate a hydride precipitate within the matrix, which manifests as a hysteresis during the thermal cycling of H loaded specimens. So, it is observed that the temperature at which the last hydride dissolves on heating is considerably higher than the temperature at which the first hydride precipitates on cooling [4,5]. Such undercooling provides part of the energy necessary to elastically and plastically distort the matrix, in order to make space for the precipitate. Hence in these metal–H systems there are two different solvus lines, with the concentration of H in solution during cooling (TSSP) being considerable higher than the concentration found at the same temperature during heating (TSSD). In general, application of an external load can provide part of this plastic work, and hence substantially reduce the hysteresis. So, a tensile stress applied during cooling along a carefully selected direction could help to accommodate the precipitates, allowing hydrides to form at a higher temperature than in the unstressed material, lowering the TSSP solvus. Equivalently, in an open system a hydrostatic tensile stress during heating expands the metal lattice, helping to accommodate the interstitial protons, bringing up the TSSD solvus.

The terminal solid solubility c^σ_s of H in solution in a closed system under uniform (external or internal) stress σ_{ij} has been theoretically analyzed by several authors [2,3,5–7],

* Corresponding author. Tel.: +54 2944 44 5154; fax: +54 2944 445299.
E-mail address: j.r.santisteban@cab.cnea.gov.ar (J.R. Santisteban).

0022-3115/$ - see front matter © 2013 Elsevier B.V. All rights reserved.
http://dx.doi.org/10.1016/j.jnucmat.2013.12.025

$$c_s^{\sigma} = A \exp\left(\frac{H_{hyd}}{RT}\right) \exp\left(\frac{W_{acc}}{RT}\right) \exp\left(\frac{W_{int}}{RT}\right), \quad (1)$$

where A is a constant, R is the gas constant, and T is absolute temperature. The enthalpy, H_{hyd}, in this expression has a large negative value and is the molar enthalpy change for transferring hydrogen from solid solution to hydride in the absence of any hysteresis effects. W_{acc}, denotes the *accommodation* energy (enthalpy), i.e. the energy change involved in elastically and plastically accommodating the transformation strain associated with hydride formation and H dissolution. W_{int} denotes the *interaction* energy change that results from the interaction of the volume change that accompanies hydride formation or dissolution under an external (or internal) stress field. Both W_{acc} and W_{int} are different for precipitation and dissolution, and their actual determination is difficult from both theoretical and experimental methods. The volume increase associated with hydride formation is relatively large, so most metals deform plastically to accommodate the hydride precipitate. Existing dislocations or slip bands within the matrix can aid hydride nucleation, by providing suitable nucleation sites and by reducing the accommodation energy W_{acc} [6,8]. Theoretical estimations of plastic accommodation are particularly difficult, so linear elastic models have been commonly used to describe the precipitation process [9,10]. In these elastic models the interaction energy term is given by,

$$W_{int} = -V_M \sigma_{ij} e_{ij}^T, \quad (2)$$

where the notation of summation over repeated indexes have been used. V_M is the partial molar volume of the metal, and e_{ij}^T represents the *transformation* strain, in the order of 5%, required to transform the metal lattice (containing dissolved H) into the hydride lattice, i.e., $e_{ij}^{H\to hyd}$. The trace of e_{ij}^T gives the relative change between the volume occupied by H in the hydride and in solid solution. Equivalently for dissolution, e_{ij}^T gives the deformation $e_{ij}^{hyd\to H}$ involved in transforming the hydride lattice into the metal lattice with dissolved H. As the H concentration at the hydride–matrix interface during precipitation and dissolution is unknown, the actual values of these transformation strains remain uncertain.

Local changes in solubility can have serious implications for in-service performance of structural components made of these hydride-forming metals. H solubility may vary across macroscopic specimens due to differences in microstructure, or as a result of external loads. Stress concentrators produce a sub-critical crack growth mechanism that involves the diffusion of H to the stressed region ahead of a crack, followed by nucleation and fracture of hydrides at the crack tip [10–13]. The phenomenon is intermittent, with the crack propagating through the hydride and stopping when it reaches the matrix. By repeating these processes, the crack propagates through a component with a velocity that depends on the rate of hydride accumulation at the crack tip, i.e., by the kinetics of hydrogen diffusion from the bulk of the material into the crack tip. The driving force for H diffusion lies in the difference between the stress state found near the crack tip and that existing in the bulk. Most research effort to understand this phenomenon has occurred within the nuclear industry where it is referred to as Delayed Hydride Cracking (DHC), as it affects the safe operation of pressure tubes (Zr2.5%Nb) and the long-term storage of nuclear fuel (Zircaloy-4 and Zircaloy-2 cladding) [13]. The interpretation of the actual stress-induced mechanisms that trigger the DHC process are still under discussion, as it has been recently reviewed by McRae et al. [14]. This is because hydrogen diffusion and hydride precipitation at the crack tip could result both from the effect of stresses on the chemical potential of H in solid solution (linked to the dilatational strain e_{ij}^H), and on the hydride precipitation solvus (linked to the transformation strain e_{ij}^T) [15].

In this work we focus on an aspect of the TSS dependence on stress that has been previously overlooked. Zr components are composed of anisotropic crystallites from a variety of orientations. The capability of a tensile load to aid or impede precipitation depends on the crystallite orientation by expressions of the form of Eq. (2), involving both strain tensors e_{ij}^H and e_{ij}^T. Hence, in general, application of an external load or the presence of intergranular stresses should result in different TSS solvi for the different families of grain orientations. Here we report synchrotron diffraction experiments performed in situ during hydride dissolution and precipitation in Zr2.5%Nb specimens under uniaxial tensile load, that reveal the effects of grain orientation and stress on hydride precipitation and dissolution temperatures; and the redistribution of H that accompanies such changes. The paper is a continuation of a previous work reporting the effect of external stresses on the crystallographic texture and stress state of hydride precipitates in Zr2.5%Nb, and their connection to hydride reorientation [16]. The actual samples and experiments are the same as the ones reported in that work. The present analysis also follows from the concepts introduced there. Although a brief description of samples, experimental arrangement and data analysis procedures are provided here, the reader is referred to Ref. [16] for additional information.

2. Samples and testing

Two sets of dog-bone tensile specimens pre-charged with different hydrogen contents were produced from commercial and experimental Zr2.5%Nb pressure tubes. Specimens E1 and E2 correspond to the normal manufacturing process for CANDU pressure tubes, whilst specimens L1 and L2 correspond to a slightly different manufacturing route being developed at CNEA, Argentina. The main difference is the use of a pilger-type *cold rolling* stage instead of the *cold drawing* stage used by AECL. The microstructure of both types of pressure tubes is essentially the same, and consists of lamellar α-grains with an *hcp* crystal structure containing between 0.6 and 1 wt% Nb, surrounded by a grain boundary network of Nb stabilized β-Zr with a *bcc* crystal structure containing about 18–20 wt.% Nb. On average, the α lamellae are ~10 μm long along the axial direction, ~1 μm wide along the hoop direction, and ~0.5 μm thick across the radial direction. Dog-bone tensile samples of 2 mm thickness were machined from the tubes with the tensile direction along the hoop direction of the tube, with the dimensions indicated in Fig. 1a. Different H contents were introduced in the specimens by cathodic charging prior to machining, followed by annealing under a N_2 atmosphere for 24 h at 400 °C. The H concentrations explored in this study are in the range between 45 and 130 wt ppm, as determined with a chromatograph LECO RH-404 with an error of ~5 wt ppm. Table 1 lists the H content measured for each specimen.

X-ray diffraction experiments were conducted at the beamline 1-ID of the Advanced Photon Source at Argonne National Laboratory [17], using the experimental arrangement schematically depicted in Fig. 1a. The tensile probes were fastened in a loading frame, and heating and cooling cycles in air under stress were applied using a lamp furnace. Diffraction rings were recorded in situ by an area detector in transmission geometry, providing information that is averaged over the full thickness of the sample. For the present experiments, we used a monochromatic incident beam of 0.15 Å wavelength and a cross section of $(300 \times 300)\ \mu m^2$. The area detector was a high speed charge coupled device (CCD) composed of 2048×2048 pixels with $200 \times 200\ \mu m^2$ pixel size located at 1948 mm from the sample. This allowed recording several full diffraction rings within a very short time (~1 s). The area detector in Fig. 1a displays an actual image captured during the experiments, after correction by dark current, flat-field and spatial distortion [17]. The terminal temperatures for hydride dissolution and precipitation were obtained from analysis of the images, as described in the next section.

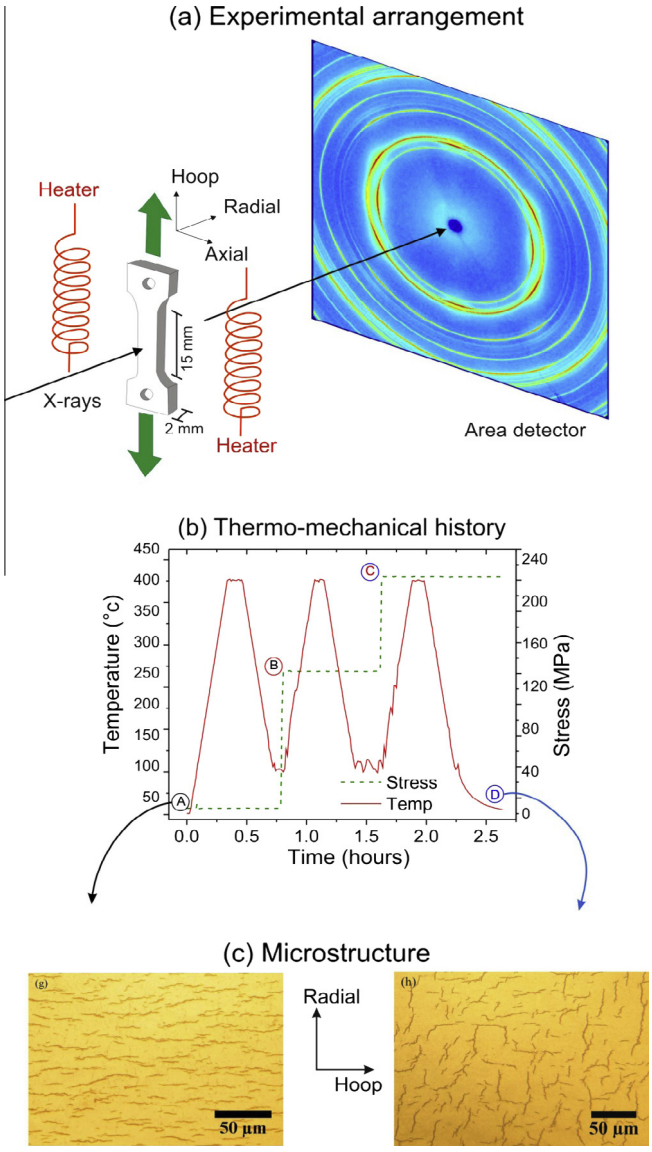

Fig. 1. (a) Schematic representation of sample geometry and experimental arrangement used for in situ X-ray diffraction during thermo-mechanical cycles. (b) Thermo mechanical history of the L2 specimen, consisting of three thermal cycles under different applied loads. Images of the Debye rings were taken every 1 s. (c) Optical micrographs showing the hydride distribution in L2 specimen before (left) and after (right) the thermo-mechanical cycle.

A typical thermal cycle is displayed by the solid [1]red line in Fig. 1b. The temperature was sensed by a thermocouple placed near the center of the gauged length of the sample. Heating and cooling rates of 20 °C/min were applied, and a maximum temperature of 400 °C was reached during the test and held at this value for ~5 min. For the H contents analyzed in this work, this temperature was high enough to completely dissolve pre-existing hydrides. For each specimen, the first heating and cooling cycle was performed without stress, but on subsequent cycles load was applied at low temperature (~90 °C), and maintained during the heating and cooling cycles. The stress on the specimen throughout the test, derived from the section of the sample and recorded load, is given by the green dotted line in Fig. 1b. Two thermal cycles were performed under loads of 125 MPa and 225 MPa to all samples, with the exception of the L1 specimen (only 56 MPa). The stress was enough to produce the reorientation of the hydride platelets, as seen in Fig. 1c, showing the distribution of hydrides in the hoop–radial plane of the L2 specimen before (left) and after (right) the thermo-mechanical treatment. Similar images for the other specimens, together with sample preparation details are given in Ref. [16]. Before testing, the sample contained almost exclusively circumferential (hoop) hydrides, i.e., platelet hydrides with the plate normal along the tube radial direction. After the tests, a considerable fraction of radial hydrides have formed (plate normal along the tube hoop direction), yet a fraction of circumferential hydrides is still clearly observed.

[1] For interpretation of color in Figs. 1 and 4, the reader is referred to the web version of this article.

3. Results

3.1. Diffracted signal and crystallite orientation

The diffraction image shown in Fig. 1a is invariant under reflections on vertical or horizontal planes, as expected from the orthorhombic symmetry of the sample. This reduces the meaningful section of the image to a single quadrant. A detail of such a quadrant is displayed in Fig. 2a, here for the L2 specimen at room temperature. The first four diffraction rings have been indexed. Three of them are clearly visible in the image, corresponding to the hexagonal α-Zr phase. The remaining ring comes from the δ zirconium hydride face centered cubic phase, barely visible due to the low H content involved. The intensity variations observed around the rings are due to the strong crystallographic texture of the material. As a result of the manufacturing process, the α-Zr phase in Zr2.5%Nb pressure tubes is composed mainly by crystallites of a limited number of orientations. These *preferred orientations* correspond to the different components of the crystallographic texture of the material, schematically represented in Fig. 2b by hexagons of different colors, in a reference system defined by the tube geometry. The crystallographic texture of pressure tubes has been thoroughly described in Refs. [18,19]. Most grains have their *c*-axes aligned along the tube hoop direction, sharply decreasing in number when the *c*-axis is tilted towards the tube radial direction. Those crystallites have been represented in the figure by three ideal orientations: (i) m_{Hoop}, in green, with the *c*-axis along the hoop direction, (ii) m_{Radial}, in red, with the *c*-axis along the radial direction, and (iii) m_{Tilted}, in blue, with an orientation between those two, tilted by 20° from the hoop direction. Besides this, there is a very small fraction of crystallites, m_{Axial}, having their *c*-axes oriented along the tube axial direction, in pink in the figure.

In order to analyze the diffraction rings, slices of the image are transformed into 2θ diffractograms, which are then processed as conventional θ–2θ scans. Fig. 2c displays the diffractograms obtained from the two slices represented in Fig. 2a. The green solid curve corresponds to the $\phi = 0°$ slice, spanning a section of ±5° around the vertical line (hoop direction). Due to the low diffraction angles involved in these experiments ($2\theta_B \sim 3°$), the diffractograms derived from the images provide information from grains having diffracting plane normals approximately within the hoop–axial plane of the tube, as seen in Fig. 1a. Hence, the α(0002) peak dominating the $\phi = 0°$ diffractogram comes from crystals having the *c*-axes of the hexagons almost parallel to the tube hoop direction, i.e., a direct manifestation of the m_{Hoop} texture component. The blue curve corresponds to the other slice, identified as $\phi = 70°$, since it is centered at an azimuth angle of 70° from the hoop direction. The α(0002) peak is absent in this diffractogram. These two slices have been chosen in order to reveal the hydride phase, as within these azimuth angles falls ~95% of the diffracted intensity registered around the δ(111) Debye ring. Hence, the hydride phase becomes clearly visible in both curves through a small δ(111) peak at ~2.75 Å, whilst much lower δ(111) intensities

Table 1
Temperatures of terminal solubility of hydrogen in Zr2.5Nb pressure tubes, obtained from high-energy X-ray diffraction experiments, for the four specimens investigated in this work. Values discriminate between hydride dissolution and precipitation in two grain orientations, and for different loads applied along the hoop direction of the pressure tube.

Sample	H (wt ppm)	Stress (MPa)	TSSP Hydrides precipitated in				TSSD Hydrides precipitated in		
			m_{Hoop}		$m_{Tilted} + m_{Hoop}$	Whole ring average	m_{Hoop}	$m_{Tilted} + m_{Hoop}$	Whole ring average
			δ(1 1 1) area (°C)	*c*-Axis (°C)	δ(1 1 1) area (°C)		δ(1 1 1) area (°C)	δ(1 1 1) area (°C)	
E1	55	0	164(3)	163(3)	164(2)	–	245(5)	258(3)	–
		125	167(5)	–	176(3)	–	232(10)	243(5)	–
		225	170(5)	–	174(3)	–	237(10)	248(5)	–
E2	67	0	194(2)	203(4)	201(2)	200(2)	257(3)	278(2)	285(10)
		125	204(3)	205(4)	205(3)	186(5)	261(2)	279(2)	270(5)
		225	207(2)	208(4)	210(2)	194(5)	265(4)	279(2)	251(10)
L1	44	0	165(5)	170(4)	170(3)	–	230(4)	258(6)	–
		56	170(5)	173(4)	171(4)	–	222(4)	244(3)	–
L2	130	0	262(2)	262(3)	270(2)	260(2)	341(3)	349(2)	345(3)
		125	270(2)	274(3)	276(2)	267(3)	326(3)	336(2)	318(3)
		225	281(2)	280(3)	279(2)	253(5)	330(3)	337(2)	310(3)

are observed at other azimuth angles (see Fig. 4b of Ref. [16]). The concentration of the diffracted signal at these azimuth angles is because hydrides precipitate with a fixed orientation relationship with the metal matrix, which itself has a strong crystallographic texture, as discussed above. Identification of the orientation of the crystallites responsible for the observed diffraction signal is essential, in order to assess the actual stress state of the α-Zr grains in which hydride precipitation takes place. In the great majority of cases δ-hydrides precipitates follow an orientation relationship that conserves close packed planes and directions with the α-Zr lattice [20], namely, $\alpha(0001)||\delta(1\,1\,1)$ and $\alpha[1\,1\,\bar{2}\,0]||\delta[1\,\bar{1}\,0]$. This is the case in the present experiment [16], hence a direct connection exists between the α(0002) and δ(1 1 1) peaks seen in the $\phi = 0°$ diffractogram of Fig. 2c. The hydrides responsible for the δ(1 1 1) peak have precipitated in α-Zr grains having their *c*-axes along the hoop direction, i.e., the same crystallites producing the α(0002) peak in that diffractogram. So, when heating the sample, the disappearance of the δ(1 1 1) peak due to hydride dissolution is accompanied by a very small increase in the α(0002) peak area. Similarly, during cooling a very small fraction of the grains producing the α(0002) peak ceases to contribute to that peak, to begin producing the δ(1 1 1) peak that reveals the presence of the hydride phase. The situation is different for the $\phi = 70°$ diffractogram. There is no α(0002) peak in this diffractogram, hence the δ(1 1 1) peak intensity must come from hydrides precipitated in α-Zr grains having their *c*-axes along other direction(s), as the δ(1 1 1) reflection has an 8-fold multiplicity. The texture analysis performed in Ref. [16] revealed two origins: (i) hydrides precipitated in α-Zr grains with their *c*-axes along the hoop direction (the same as those in the $\phi = 0°$ diffractogram); and (ii) hydrides precipitated in α-Zr grains with their *c*-axes having directions intermediate between the hoop and radial directions of the tube, centered at ∼20° from the tube hoop direction, the m_{Tilted} grains in Fig. 2b. This explains the observation that the δ(1 1 1) intensity in the $\phi = 70°$ diffractogram is nearly twice that in the $\phi = 0°$ diffractogram (refer to the results for L2 specimen in Table 1 of Ref. [16]). From this analysis, it is expected that the effect of the applied stress on hydride precipitation will have different impact on the δ(1 1 1) peaks of these two diffractograms.

A direct manifestation of the effect of the applied stress on hydride precipitation is displayed in Fig. 3, showing detail of (a) $\phi = 0°$ and (b) $\phi = 70°$ diffractograms registered at 270 °C during cooling of the L2 specimen with and without external loads. No hydride peak is observed in either of the diffractograms when cooling proceeds without load (black solid symbols), yet a clear δ(1 1 1) peak emerges (red empty symbols) when a load of 225 MPa is applied along the hoop direction. The appearance of the δ(1 1 1) peak at 270 °C under load when no peak is observed without load plainly demonstrates that hydride precipitation in Zr2.5%Nb is affected by external stresses. Yet, the effect of stress on precipitation is not large and it depends on crystallite orientation, so it could be easily missed out by other data analysis strategies. To see this, Fig. 3c shows a detail of the diffractograms obtained by integrating the counts registered around the *full* diffraction rings. The δ(1 1 1) peak that appears under load is almost lost due to the deterioration of the signal-to-noise ratio, hindering detection of the effect of stress in the full ring diffractograms. This means that the effect of stress may be very difficult to see in any experiments using other experimental techniques such as dilatometry, dynamic elastic modulus, or internal friction, since these methods derive their response from hydride formation and dissolution of all crystallite orientations.

The temperatures corresponding to the terminal solid solubility for dissolution (TSSD) and for precipitation (TSSP) of hydrides can be defined by following the dependence of the δ(1 1 1) peak intensity on temperature during the heating and cooling ramps, respectively. Fig. 4a shows the evolution of the δ(1 1 1) peak area from the m_{Hoop} diffractogram, registered during the first thermal cycle of the L2 specimen with no load applied. The solid red symbols correspond to the heating stage, and the open blue symbols to the cooling stage. The plotted peak area values were derived from least-squares refinements of the diffractograms within the d-space interval displayed in Fig. 3, using a two-peak fitting profile. The small gaps existing between the data points in Fig. 4a are due to the dead time required to store the images captured by the CCD. A clear hysteresis is observed between dissolution and precipitation, but the area of the δ(1 1 1) peak remains unchanged after completion of the thermal cycle. The δ(1 1 1) peak area provides direct information about the hydrides precipitated within the m_{Hoop} grains. The inflexion point observed in the heating curve for zero peak area at ∼340 °C tell us the temperature at which the hydrides in the m_{Hoop} grains were completely dissolved, i.e., when there was no more hydrogen that could be transferred *from* the precipitates into the Zr matrix. This defines the temperature at which the terminal solid solubility is attained (TSSD) in these grains. The equivalent inflexion point in the cooling curve at ∼260 °C indicates the temperature at which hydrogen starts to be transferred from the Zr matrix *into* hydrides that are precipitated within the m_{Hoop} grains, hence defining the temperature at which the terminal solid solubility (TSSP) starts

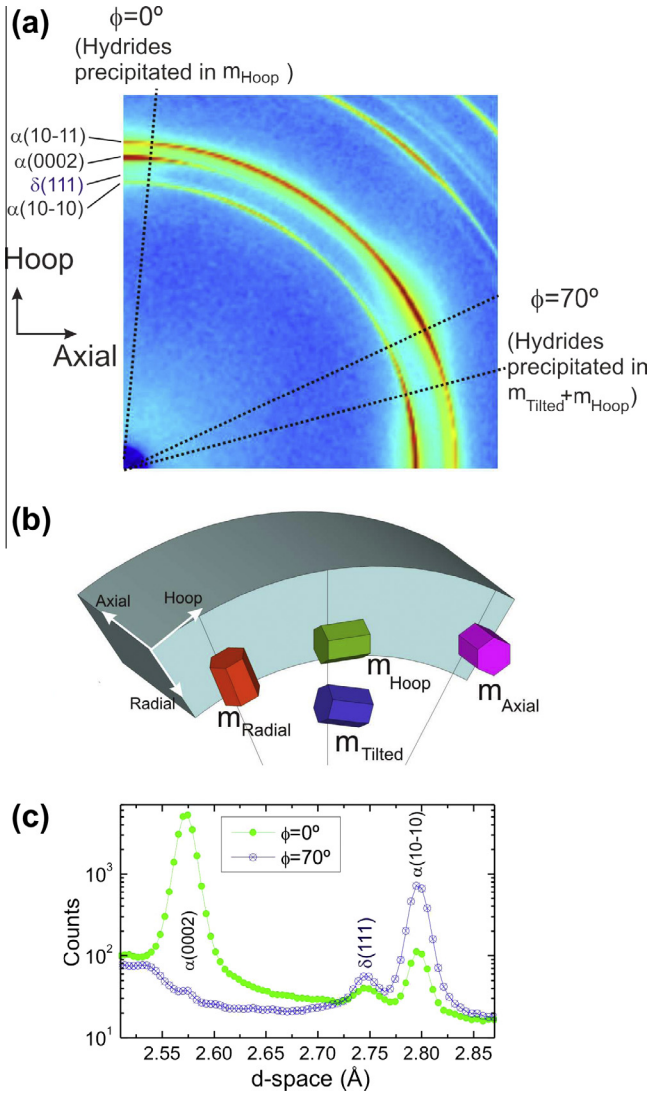

Fig. 2. (a) Detail of typical Debye rings captured by the CCD in Fig. 1a, with the first four rings indexed. Intensity variations around the ring are due to strong crystallographic texture of the material. (b) Ideal texture components of α-Zr phase in pressure tubes. (c) Diffractograms obtained from the two azimuth sections identified in figure (a). The green curve provides information from hydrides precipitated in α-Zr grains of m_{Hoop} orientation, represented in figure (b). The blue curve gives information from hydrides precipitated in grains of both m_{Hoop} and m_{Tilted} orientations. (For interpretation of the references to color in this figure legend, the reader is referred to the web version of this article.)

decreasing. The inflexion points indicating the TSSD and TSSP temperatures were defined by extrapolating the heating and cooling curves respectively, to find the intersection with the horizontal line corresponding to area = 0. The temperatures for TSSD, (341 ± 3) °C, and for TSSP, (262 ± 2) °C, obtained for the thermal cycle in the figure are represented by vertical dotted lines. The uncertainty in the TSSP temperature is smaller than that in the TSSD temperature because the cooling curve has a sharper slope than the heating curve. The values for the TSSP and TSSD temperatures are close to the value measured for this material and H concentration by differential dilatometry (DD), but lower that values obtained from other experimental techniques [21].

Direct information about the concentration of hydrogen actually dissolved within the metal matrix can be obtained by following the dependence of the α-Zr lattice parameters with temperature, as recently investigated by Zanellato et al. for H in Zircaloy-4 [22]. The hexagonal lattice is (anisotropically) expanded when interstitial hydrogen enters into it [23]. Hence the change with temperature of the lattice parameters gives a measure of the amount of H in solution, provided other effects contributing to the lattice expansion are properly accounted for. Fig. 4b shows the evolution of the *c* lattice parameter of the L2 specimen for the same thermal cycle as given in Fig. 4a, obtained by least-squares fit of the α(0002) peak of the m_{Hoop} diffractograms. The hysteresis loop reveals the difference in H concentrations in solution found during heating and cooling of the specimen. Inflexion points are observed at approximately the same temperatures observed in δ(111) curves, confirming the previous interpretation. Hence, the figure provides an independent determination of the TSSP and TSSD temperatures, as sensed by changes in the lattice spacing of the α-Zr lattice. The hysteresis loop appears on top of the linear increase of the lattice parameter due to thermal expansion, indicated by dotted lines in the figure. The inflexion points are better defined by subtracting the thermal expansion from the measured lattice parameter (Fig. 4c). After this operation, the temperature corresponding to the beginning of precipitation can be precisely defined by finding the intersection of the lines describing the approximately straight line sections at both sides of the inflexion point, as shown in the figure. The temperature corresponding to the end of dissolution is harder to define, as the change in slope is not so sharp for this case. It is important to note that the height of the step observed in the lattice parameter (Δ*c* in the figure) gives a direct measure of the amount of H that has ceased to be in solid solution within the m_{Hoop} grains during cooling, i.e., that has been expelled from the α-Zr matrix.

3.2. Effect of external stress on hydride precipitation

Fig. 5 displays the effect of an external stress on the hydride precipitation process, again, for m_{Hoop} grains of the L2 specimen. The top figure compares the evolution of the δ(111) peak area measured without load (open symbols) with the values obtained when a 225 MPa load was applied along the tube hoop direction during precipitation (solid symbols). The open-symbol curve is identical to the cooling curve presented in Fig. 4a, but the temperature axis has been inverted in order to give a sense of the direction in which hydride precipitation has proceeded. The bottom figure displays the deformation of the *c*-axis of the α-Zr unit cell due to dissolved H, expressed in terms of a strain, as explained in Fig. 4c. Two main results emerge directly from the figure: (i) application of the load produces a considerable increase in the number of hydrides precipitated in crystals with m_{Hoop} orientation, (ii) the temperature at which hydrides start to precipitate in these grains is increased from ~260 °C to ~280 °C, i.e., during cooling hydrides begin precipitation ~20 °C before than in the unloaded condition. Besides this, there is another not so evident yet very important result: (iii) the height of the step observed in the *c*-axis strain is essentially the same with and without an applied load. This means that the amount of H in solution within m_{Hoop} grains at 400 °C remained nearly constant, even when the 225 MPa load was applied during the 5 min hold up period (Fig. 1b).

In order to quantify these findings, on the right side of the figures the diffraction results have been expressed in terms of the H content responsible in producing the measured signals. To quantify the H present as a hydride we have compared the areas of the δ(111) and α(0002) peaks, using a slightly modified version of the expression presented in Ref. [24] for calculation of the volume fraction of each phase. This is because that work assumed a polycrystalline specimen with random orientations for both the α-Zr and δ-hydride phases, which is clearly not applicable to the present study. So, the multiplicity factor appearing in Eq. (2) of Ref. [24] is absent here because the δ(111) and α(0002) planes measured by the hoop diffractogram are directly connected, as

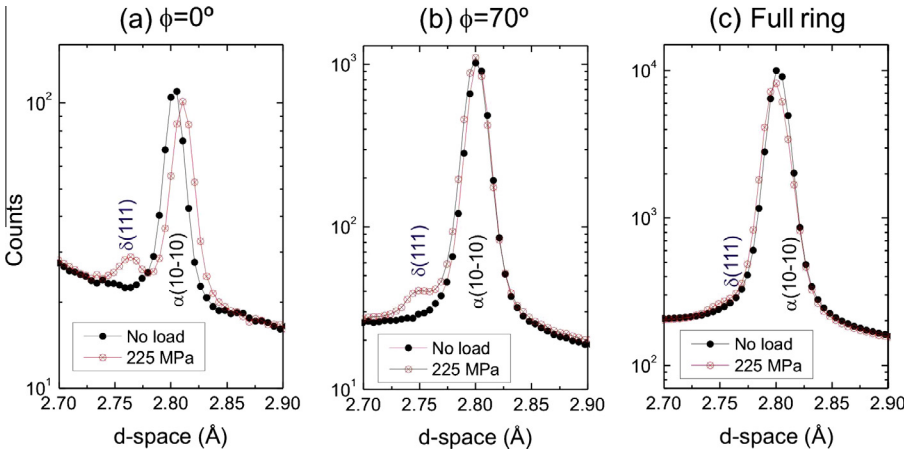

Fig. 3. Detail of diffractograms recorded at 270 °C during cooling of L2 specimen with and without an applied load, showing the effect of stress on hydride precipitation. (a and b) Diffractograms obtained from the azimuth sections of Fig. 2, with hydride precipitates clearly visible under load but absent in the unloaded condition. (c) Diffractograms obtained by integrating the counts registered around the full diffraction ring, where the hydride phase present under load becomes almost invisible.

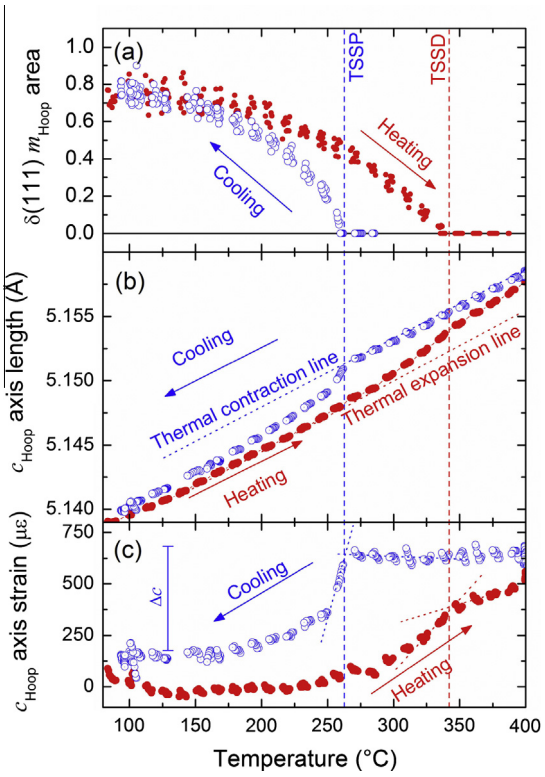

Fig. 4. Evolution of selected crystallographic variables during the first heating and cooling cycle of L2 specimen, obtained from the m_{Hoop} diffractogram. (a) δ(111) peak area, (b) *c* lattice parameter of hexagonal α-Zr phase. Inflexion points in the curves indicate the temperature when hydride dissolution ends (TSSD), and when hydride precipitation begins (TSSP). (c) Inflexion points are better defined after subtraction of thermal expansion from the evolution of the *c* lattice parameter.

explained in the previous section. On the other hand, the concentration of H in solution has been estimated using the coefficient of expansion of the *c*-axis of α-Zr when adding H in solution from an external source $\left(\frac{1}{c}\frac{dc}{dC_H} \sim 5\frac{\mu\varepsilon}{\text{wt ppm H}}\right)$ reported in Ref. [23]. Both the H content present *as a hydride* and dissolved *in solution* have been expressed in terms of ppm by weight, the usual practice for this system. The fairly good agreement between the H content measured with the LECO RH-404 chromatograph reported in Table 1 (130 wt ppm H), with the concentration obtained in Fig. 5b when all H is in solution (~120 wt ppm H for $T > 280$ °C) gives confidence to the present analysis. Comparison between both graphs reveals that in the unloaded condition just a fraction of the H found in solution in m_{Hoop} grains actually precipitates within the same grains. So, on cooling without load some H in solution in m_{Hoop} grains must precipitate in α-Zr grains of other orientations, provided the overall H content remains constant. On the other hand, the results show that application of a load changes the precipitation temperature for m_{Hoop} grains, and increases the number of hydrides precipitated within them.

Similar results were observed for all samples and applied loads. Table 1 lists the TSSP and TSSD temperatures resulting from the analysis of the δ(111) peak as discussed above, distinguishing between values obtained from the m_{Hoop} and $m_{Tilted} + m_{Hoop}$ diffractograms. For illustration, we have also included the temperatures that would be obtained from an analysis of the full-ring diffractograms, i.e., by integrating the counts registered around the complete ring. Most TSSP and all TSSD temperatures were obtained from the evolution of the hydride δ(111) peak area on temperature. The TSSP temperatures resulting from the analysis of the lattice expansion are only listed for the m_{Hoop} diffractogram. The error of this method proved too large when applied to TSSD temperatures. Fig. 6 provides a graphical representation of the table, showing precipitation temperatures in open symbols and dissolution temperatures in solid symbols, for all samples and loads. Red symbols correspond to hydrides precipitated in grains of m_{Hoop} orientation, and black symbols to those precipitated in grains of $m_{Tilted} + m_{Hoop}$ orientations. A clear difference emerges between the dissolution temperatures of the two groups. For all specimens, TSSD temperatures in the $m_{Tilted} + m_{Hoop}$ grains are consistently higher (~15 °C) than the corresponding temperatures measured in the m_{Hoop} grains. Provided that crystals of the m_{Hoop} orientation belong to both groups, this means that hydrides precipitated in m_{Tilted} grains dissolve at higher temperatures than those in m_{Hoop} grains. On the other hand, the temperatures for hydride precipitation are similar in both groups of grains, yet a difference is observed in the unloaded condition, with slightly higher precipitation temperatures (~5 °C) for the $m_{Tilted} + m_{Hoop}$ grains than for m_{Hoop} grains. This indicates that when cooling a specimen without load, precipitation at m_{Tilted} grains begins *before* that in m_{Hoop} grains. At 225 MPa precipitation temperatures measured for the m_{Hoop} and $m_{Tilted} + m_{Hoop}$ coincide. Again, as the m_{Hoop} orientation belongs to both groups, we can only asses that at this load the precipitation temperature in m_{Tilted} grains is lower or equal to that in m_{Hoop} grains.

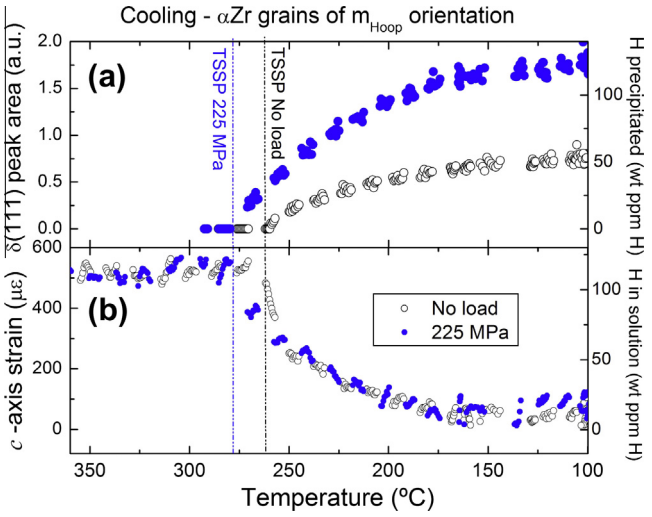

Fig. 5. Effect of stress on hydride precipitation within grains of m_{Hoop} orientation of the L2 specimen: (a) δ(1 1 1) peak area, providing the amount of H present as hydride, (b) *c* axis strain, providing the amount of H in solution in α-Zr phase. The applied load shifts precipitation towards higher temperatures, and largely increases the number of hydrides precipitating on grains of the m_{Hoop} orientation. The concentration of H in solution in m_{Hoop} grains is not affected by the application of the load.

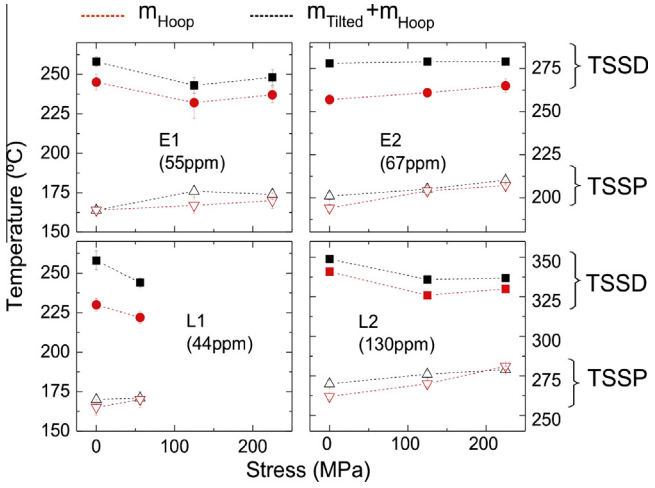

Fig. 6. Dependence of hydride dissolution (TSSD) and precipitation (TSSP) temperatures on applied stress for all specimens investigated. Load was applied along the pressure tube hoop direction. Values are discriminated for hydrides precipitated in α-Zr grains of the orientations represented in Fig. 2a.

Although the effect of stress on hydride precipitation and dissolution temperatures is not particularly large, a systematic change in precipitation temperatures clearly emerges from Fig. 6. For all samples and for the two grain orientations investigated TSSP temperatures increase on application of a load along the tube hoop direction. The change in precipitation temperature is larger for hydrides precipitated in m_{Hoop} grains than for those precipitated in $m_{Tilted} + m_{Hoop}$ grains. This is revealed by the average slopes extracted from the plots, (0.08 ± 0.02) °C/MPa for m_{Hoop} grains and (0.04 ± 0.01) °C/MPa for $m_{Tilted} + m_{Hoop}$ grains. Microscopically, the stress along the *c*-axis of α-Zr crystals is larger for m_{Hoop} grains than for m_{Tilted} grains. On the other hand, the effect of stress in dissolution temperatures is more erratic than in precipitation, mostly due to the larger uncertainty found in these measurements. Yet a general tendency towards a reduction in dissolution temperature with stress can be inferred from the figure. The exception is the E2 specimen which shows an increase for m_{Hoop} grains and no variation for the $m_{Tilted} + m_{Hoop}$ grains. As a result of these shifts, the hysteresis between dissolution and precipitation temperatures is reduced for all samples, with a maximum reduction of 30 °C for the L2 specimen.

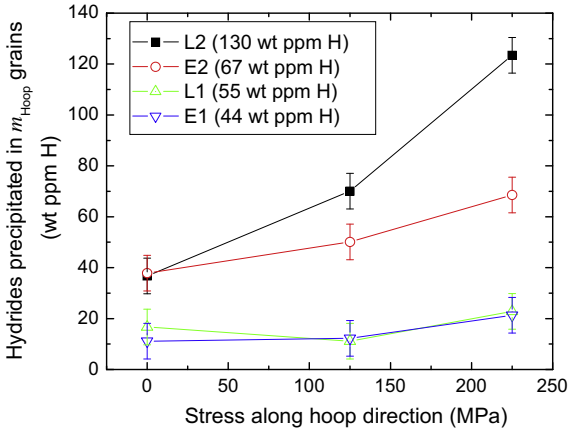

Fig. 7. Dependence of the number of hydrides precipitated within grains of the m_{Hoop} orientation on applied stress for all specimens investigated. Application of a load along the *c*-axis of the grains largely increases the number of hydrides precipitated within such grains.

Fig. 7 shows the influence of the applied load on the number of hydrides precipitated in crystals of the m_{Hoop} orientation. For all specimens investigated precipitation in the unloaded condition results in only small fraction of the available hydrogen in solution being precipitated in grains of this orientation (between 35% and 45%). Application of the load increases precipitation on these grains, particularly for the samples with higher H contents (L2 and E2).

4. Discussion

We have investigated the effect of stress on H redistribution and hydride precipitation in Zr2.5%Nb pressure tubes by synchrotron X-ray diffraction experiments performed in situ during thermal cycles. The material investigated (and all Zr-based alloys used in the nuclear industry) is mainly composed of hexagonal α-Zr crystallites having a distribution of orientations. The texture analysis of the hydride phase performed in Ref. [16] provided us the tools to *selectively* follow the precipitation and dissolution of hydrides occurring only in α-Zr crystallites within a narrow range of orientations, namely, grains having their *c*-axis within ±5° from the hoop direction of the tube. These so-called m_{Hoop} grains (identified in green in Fig. 2b) represent the largest component of the crystallite orientation distribution function (ODF) – about 60–65% of all of the grains in the α-Zr phase [18]. Besides these grains, we were also able to investigate hydride precipitation in grains from another texture component, the m_{Tilted} grains, which have orientations equivalent to a 20° rotation about the axial direction from the m_{Hoop} grains (identified in blue in Fig. 2b). The disappearance of the diffraction signal from the δ(1 1 1) hydride planes when heating the specimens marked the temperature at which hydrides were completely dissolved, independently for each of the two grain families (TSSD temperatures). Similarly, the appearance of this diffracted signal during cooling marked the temperature when hydrides begin to precipitate within the grains of each orientation (TSSP temperatures).

4.1. Dependence of dissolution and precipitation temperatures on grain orientation

The TSSD temperatures displayed in Fig. 6 clearly reveal that for all specimens investigated the hydrides precipitated in α-Zr grains of m_{Tilted} orientations dissolve at temperatures consistently higher than those in grains of m_{Hoop} orientations, with differences ranging between 8 °C and 25 °C. On the other hand, differences between precipitation temperatures are considerably smaller. Except for the E1 specimen, in the unloaded condition hydrides precipitate in m_{Tilted} grains at slightly higher temperatures (~7 °C) than in m_{Hoop} grains; yet this difference disappears upon application of the largest load. The observed values provide quantitative estimates for the span of dissolution and precipitation temperatures to be encountered in polycrystalline α-Zr specimens for different grain orientations. Such differences have been proposed to explain the broad signals observed for polycrystalline specimens (when compared to single crystals) of determinations of TSS temperatures using a low-frequency flexure pendulum [25]. The dependence of TSSD on grain orientation also explains part of the large broadening observed on dissolution signals (as compared to precipitation signals) in other macroscopic techniques that derive their signal from the bulk of the material investigated (DSC, DEM, IF, etc.) [13].

The differences in precipitation and dissolution temperatures between grains of different orientations should be taken into account on TSS determinations by directional techniques that sample only a fraction of the crystallites composing a sample. This includes diffraction (spanning a reduced solid angle) [26] and dilatometry [27]. For instance, the dissolution temperatures reported here are substantially lower than those given by isotropic bulk techniques. This could be due to the late dissolution (higher temperature) of hydrides precipitated in grains not observed by the present experimental arrangement, e.g., the m_{Radial} grains in Fig. 2b. For dilatometry, the connection between the microscopic changes reported here and the macroscopic elongation of a sample produced along a given direction is not straightforward, as discussed in Ref. [27]. The macroscopic elongation has contributions from all crystallographic phases (α-Zr, β-Zr, hydrides), and is greatly affected by the *macroscopic* morphology of the hydride clusters (Fig. 1c).

The range of dissolution temperatures is much wider than the range of precipitation temperatures, which is considered to be the result of intrinsic differences between the two processes. The initial state for heating consists of a variety of different hydrides, unevenly distributed between crystals of different orientations. As discussed in Ref. [16], hydrides precipitated in different grain orientations present morphological differences in size, shape, and internal sub-plate structure, as well as being subjected to different internal stress states. All of these factors influence the dissolution process, resulting in a wide range of dissolution temperatures. By contrast, the initial state for cooling consists of H in solution, homogeneously distributed among crystals of all grain orientations, and precipitation proceeds quite rapidly once the nucleation barrier is exceeded within a grain. Grains of different orientations may have different shapes, dislocation substructures [19], and stress states [8]. All of these factors impact on the undercooling required for producing a nucleus of critical size. Hence nucleation begins preferentially in grains of a particular orientation (m_{Tilted}), yet the associated differences in Gibbs free energy are likely small and thus could be overridden by external stresses, as discussed in the next section.

4.2. Effect of applied stress on precipitation and dissolution temperatures

A change in TSS is in general expected due to the interaction between the volume change accompanying hydride formation and the external stress field. Fig. 6 reveals a clear increase in precipitation temperature due to the applied stresses in both grain orientations, confirming that a tensile stress aids hydride precipitation in these grains. The temperature shift is larger for hydrides precipitated in m_{Hoop} grains, (0.08 ± 0.02) °C/MPa, so for a load of 225 MPa both precipitation temperatures become almost equal. This suggests that the differences in precipitation temperatures within α-Zr grains of m_{Hoop} and m_{Tilted} orientations observed without load could in principle be explained by differences in the crystallites stress state. However, internal stresses should manifest experimentally as differences in interplanar distances measured along different directions, which have not been observed in the present case. In Fig. 10 of Ref. [28] we presented the variation of the *c* lattice parameter *c* of the α-Zr unit cell on the hoop–radial plane for commercial pressure tube material, which contains the m_{Tilted} and m_{Hoop} grains discussed here. All measured values are within (5.1468 ± 0.001) Å which represents a variation of only $\sim 200\mu\varepsilon$, equivalent to a uniaxial load of ~20 MPa. A more plausible reason for the difference could be found in the dislocation substructure of the grains. Holt and Zhao [19] reported that m_{Hoop} grains have low dislocation densities, whilst m_{Radial} grains have high density of *a* and *c* + *a* dislocations. Hence, it could be expected that m_{Tilted} grains, in between these two grain orientations, would have considerable larger dislocation densities that m_{Hoop} grains.

On the other hand, the dependence of dissolution temperatures with stress is more erratic (Fig. 6), revealing a much lower correlation with applied stress than precipitation temperatures. This is in agreement with the proposed explanation that different dissolution temperatures observed for hydrides in m_{Hoop} and m_{Tilted} grains are due to morphological differences between hydrides precipitated in those grain families. As seen in Fig. 1c, the applied stress produces changes in the hydride morphology observed on a macroscopic scale, with a large increase in the fraction of radial hydrides in detriment of circumferential hydrides. Accompanying this, there is a redistribution of hydrides at the grain level, with an increase in the number of hydrides precipitated in Zr grains of m_{Hoop} orientation, yet with these hydrides still less than those in m_{Tilted} grains [16]. Such changes will affect the details of the dissolution process, hence producing an indirect impact on the dissolution temperatures of both hydride groups. So, changes in dissolution temperature will depend on the differences in morphology and stress state between the hydrides obtained with and without external load. This turns rationalization more difficult, as a large number of physical factors affect the morphology and stress state of hydrides precipitated in Zr alloys, as discussed in Ref. [16] for the present specimens.

4.3. Hydrogen nucleation and redistribution during precipitation

According to classical nucleation theory, the rate of appearance of nuclei able to overcome the nucleation barrier is $I \sim \exp(-\Delta G^a/kT)$, with ΔG^a the activation free energy barrier. This energy barrier includes the chemical energy difference between the matrix and precipitate, the energy required to create the new surface and the strain energy resulting from the misfit between the nucleus and the matrix. Preferential nucleation occurs in some part of a solid because of local conditions that lower the nucleation barrier, due to an increase in H concentration there (and, hence in the chemical driving force) and/or a reduction in the positive strain energy term. If these sites maintain their advantage during cooling, they continue to act as preferential nucleation sites throughout the cooling period, thereby increasing the number of precipitates formed in such regions. Hence, cooling of a polycrystalline specimen containing H in solution (equally distributed among grains in the unloaded condition) will result in an increase in H content within the grains where hydrides precipitate first. In Ref. [16] we concluded

that hydrides in pressure tubes precipitate mostly in grains of m_{Tilted} orientation. In agreement with that, here we have found that in the unloaded condition hydrides precipitate in m_{Tilted} grains at slightly higher temperatures than in m_{Hoop} grains. We have also observed that precipitation temperatures can be modified by application of an external load (Fig. 6), increasing the probability of precipitation within those groups of grains in which the net change in interaction energy due to external load (Eq. (2)) is most negative. The large increase in the number of hydrides precipitated in m_{Hoop} grains shown in Fig. 7 is in direct agreement with the increase in precipitation temperatures observed in Fig. 6.

Details about how H redistributes among different grains can be inferred from Fig. 5. In the unloaded condition there is about 120 wt ppm of H in solution within m_{Hoop} grains (open symbols in Fig. 5b), and after cooling only ~50 wt ppm is present as hydrides within these grains (Fig. 5a). This means that during cooling in the unloaded condition ~70 wt ppm of H have left the m_{Hoop} grains to precipitate as hydrides in other grains, presumably in m_{Tilted} grains. This confirms that H redistribution occurs essentially during precipitation, mainly due to the diffusion of H from grains with lower precipitation temperatures into grains with higher precipitation temperatures. Diffusion of H between neighboring grains is fast at the TSSP temperatures studied here. For a typical diffusion length of 1 μm, diffusion times range from 0.01 s at 270 °C to 0.08 s at 165 °C, which are fast compared with the cooling rate of ~0.3 °C s^{-1} used in the present experiments. The situation changes upon application of the load, because the load aids hydride nucleation in grains having their *c*-axes aligned with the load direction, and precipitation within m_{Hoop} grains starts now at a higher temperature than in the unloaded condition. Hence, under a 225 MPa load, the 120 wt ppm of H dissolved in m_{Hoop} grains has presumably all precipitated within the same grains.

Two physical mechanisms could be responsible for preferential hydride nucleation in uniaxially stressed m_{Hoop} grains. The external load could help accommodation of the hydride and hence lower the nucleation barrier, and/or it could increase the concentration of dissolved H within these stressed grains, hence reducing the chemical driving force required for nucleation. Redistribution could occur while H is in solution because the anisotropy of e_{ij}^{H} means that a uniaxial external load has different impact on the chemical potential of H atoms dissolved in differently oriented grains. Equilibrium between these differently oriented grains subjected to the same uniaxial stress is achieved when the chemical potentials of H in these different groups are equal. Kirchheim and Hirth have given a derivation for the differences in H concentrations for such a case in a cubic crystal with random crystal orientations and tetragonally misfitting H atoms [29]. A calculation applied to the present case considering the texture of Zr2.5%Nb tubes shows that this difference in concentration is, however, extremely small (<1 wt ppm) for an applied tensile stress of 225 MPa. This is in agreement with Fig. 5b, which shows that there is no detectable difference in dissolved H concentration as a result of the application of an external load. Such change in H concentration would result in an increase of ~0.7 °C in precipitation temperature within m_{Hoop} grains (as derived from the precipitation solvus), much smaller than the ~20 °C observed in the present experiments. Hence, the main reason for preferential nucleation within m_{Hoop} grains upon application of the load would be that an external stress modifies the precipitation solvus because it helps in accommodating the volume change associated with hydride precipitation, as discussed in the next section.

4.4. Theoretical models of stress effects on precipitation temperatures

The effect of stress on hydride precipitation temperatures in Zr2.5%Nb is important for proper understanding of the DHC process in CANDU pressure tubes. Hence several studies have discussed models to quantify this effect ([13–15] and references therein). In particular, Refs. [30–32] have calculated the shift in TSSP temperature on the basis of these models. The values estimated are considerably lower than the present experimental results. Using a simple isotropic model and the volume per H in α-Zr and δ-hydride known at the time, Coleman and Ambler [30] predicted a change of 0.015 °C/MPa. In a later work, Eadie and Coleman [31] included the effect of the anisotropic strain involved in the α–δ transformation, and used more precise values of the volume per H, predicting a value of 0.0006 °C/MPa. Finally, Shi [32] considered the specific case explored in the present experiments, of Zr2.5%Nb pressure tube material uniaxially loaded along the hoop direction, for stresses large enough (>200 MPa) to produce hydride reorientation. Moreover, the calculation was performed precisely for hydride precipitation in α-Zr crystals having their *c*-axes along the tube hoop direction, in exact correspondence with the m_{Hoop} grains studied in this work. Shi's calculation estimated a change of 0.0003 °C/MPa, about two orders of magnitude smaller than the (0.08 ± 0.02) °C/MPa value derived from Fig. 6. All of the foregoing calculations were based on the assumption that undercooling is reduced because part of the plastic work required for the transformation to occur is provided by the work ΔW performed by the external load. Hence the actual precipitation temperature is changed by a value $\Delta T = \Delta W/\Delta S$, with ΔS the entropy change involved in the transformation. In those studies, the work ΔW was estimated as the interaction energy given in Eq. (2), using different numerical values for the transformation strain e_{ij}^{T} between the α-Zr and δ-hydride phases. A value for the work, $\Delta W = \Delta T \cdot \Delta S$, can be directly evaluated here from the experimental shift in precipitation temperatures and a theoretical model for the entropy change. This change is usually approximated by the entropy of the solid solution,

$$\Delta S = R \ln(A/C_H), \tag{3}$$

where C_H is the H concentration, and A has been defined in Eq. (1). Using $\Delta T = (0.08 \pm 0.02)$ °C/MPa, we obtain $\Delta W = (780 \pm 150)$ J/mol. A more detailed model for the entropy change has been proposed by Shi [32], which includes the stoichiometry of the hydrides,

$$\Delta S = R \frac{x}{1+x} \ln(A/C_H). \tag{4}$$

So, in this expression estimation of the entropy requires knowledge of the composition x of the hydrides involved in the phase transformation ($Zr + xH \leftrightarrow ZrH_x$) that occurs at the hydride–matrix interface. As we have only observed δ-peaks during precipitation, the hydride composition should lie near the α + δ/δ line of the phase diagram [33]. For the precipitation temperatures explored in the present experiments (160–280 °C) the composition x of the δ phase would be between 1.45 and 1.5, obtaining a value of $\Delta W = (470 \pm 100)$ J/mol. Using Eq. (2), the transformation strain e_{ij}^{T} can be directly evaluated from the estimated ΔW and the value of the applied stress σ_{ij}. For m_{Hoop} grains the value of e_{ij}^{T} is measured along the *c*-axis, which corresponds to e_{33}^{T} in the base defined by $x_1 = [1\,\bar{2}\,1\,0]$, $x_2 = [1\,0\,\bar{1}\,0]$ and $x_3 = [0\,0\,0\,1]$. So, we obtain values of $e_{33}^{T} = (0.25 \pm 0.05)$ from the simple entropy change given by Eq. (3), and $e_{33}^{T} = (0.15 \pm 0.03)$ from the more complex model given by Eq. (4).

Theoretical estimations of ΔW in Refs. [30–32] have been based on a model introduced by Puls [2] to explain the solubility of H observed in several metals. Such model explains how the chemical (incoherent) solvus is shifted in a finite solid under external stress, where precipitation of a second phase results in coherency stresses that can be partially reduced by plastic deformation, i.e., the source of hysteresis between hydride precipitation and dissolution. The model has evolved over the years [2,3,13], and the derivation of the most recent version has been detailed in Ref. [13], which gives the change in work (interaction energy) for a closed system as

$$\Delta W = -V_{Zr}\sigma_{ij}e^T_{ij} = -V_{Zr}\sigma_{ij}\left[\frac{e^{hyd}_{ij}}{x} - e^H_{ij}\right], \quad (5)$$

where e^{hyd}_{ij} is the transformation strain necessary to convert the original α-Zr lattice (without H) into the Zr sub-lattice of the hydride. As described in the Introduction e^H_{ij} is the *dilational* strain, describing the expansion of the α-Zr lattice to be expected if a mole of H could be kept in solution within a mole of α-Zr. Estimations for the values of e^H_{ij} and e^{hyd}_{ij} at the temperature and concentration at which the transformation takes place can be obtained from experiments. MacEwen et al. [23] measured the dilation of α-Zr due to D in solution for concentrations $x \leqslant 0.028$, obtaining values of $e^H_{11} = e^H_{22} \approx 0.033$, and $e^H_{33} \approx 0.054$, and a D partial molar volume of $(1.67 \pm 0.17) \times 10^{-6}\,m^3$. There is no consensus in literature about the actual values of the transformation strains e^{hyd}_{ij} between the α-Zr and δ-hydride phases, and two models have been proposed for the strains required that would satisfy the orientation relationship $\alpha(0\,0\,0\,1)//\delta(1\,1\,1)$ and $\alpha[1\,1\,\bar{2}\,0]//\delta[1\,\bar{1}\,0]$ and the observed volume expansion [13]. The theoretical estimations discussed above [31,32] adopted a model proposed by Carpenter [20], with a transformation strain that is solely derived from the lattice parameter differences between the two cells (i.e., a pure lattice strain transformation), which gives (in the same base as before)

$$e^{hyd}_{ij} = \begin{pmatrix} \Delta & 0 & 0 \\ 0 & \Delta & s/2 \\ 0 & s/2 & \Delta+\eta \end{pmatrix}, \quad (6)$$

where $s = 0.36$, $\Delta = 0.0458$ and $\eta = 0.0262$ at room temperature. Estimation of the volume occupied by a proton in the hydride depends on the hydride lattice parameters and composition x, so for δ hydrides the values of Δ, η and s are somehow uncertain and depend on temperature. Puls has recently estimated the partial molar volume of H in δ hydride – determined from the temperature dependence of Δ and η for the α + δ/δ line and assuming a pure strain transformation –, by a re-evaluation of literature data (Table 2.1 in Ref. [13]). For 280 °C, we have $x \sim 1.47$ and the H molar volume is $\sim 1.77 \times 10^{-6}\,m^3$, derived from values $\Delta \sim 0.05$ and $\eta \sim 0.025$, which are not far from the transformation strains evaluated at room temperature. Both the molar volume and the diagonal strains per H atom $\frac{e^{hyd}_{11}}{x} = \frac{e^{hyd}_{22}}{x} \approx \frac{0.05}{1.47} = 0.034$ and $\frac{e^{hyd}_{33}}{x} \approx \frac{0.075}{1.47} = 0.051$ are very close to the values of the dilation strains due to H in solution, $e^H_{11} = e^H_{22} = 0.033$, and $e^H_{33} = 0.054$, reported by MacEwen et al. [23]. From Eq. (5), we realize that for these transformation strains, $e^T_{11} = e^T_{22} \approx 0.001$ and $e^T_{33} \approx 0.003$, very far from the lowest experimentally estimated value of $e^T_{33} \approx 0.15$ obtained from the measured ΔT and the entropy change given by Eq. (4). Hence, within this model the work done by the external load during the transformation would be very small, and precipitation temperatures have little dependence on applied stress, as it was indeed concluded by the theoretical models mentioned above [30–32].

On the other hand, by analogy with the formation of γ hydride, Weatherly [34] proposed a martensitic transformation (i.e., an invariant plane strain transformation) with the habit plane very close to {10–17} and volume expansion accommodated normal to that plane. Using the same notation this gives,

$$e^{hyd}_{ij} = \begin{pmatrix} 0 & 0 & 0 \\ 0 & 0 & s/2 \\ 0 & s/2 & 3\Delta+\eta \end{pmatrix}, \quad (7)$$

which gives diagonal strains per H atom values $\frac{e^{hyd}_{11}}{x} = \frac{e^{hyd}_{22}}{x} = 0$ and $\frac{e^{hyd}_{33}}{x} \approx \frac{0.175}{1.47} \approx 0.12$. This results in a value of $e^T_{33} = 0.066$, more than 20 times larger than the calculated above, and in the same order of magnitude of the experimentally estimated value. The calculated value is highly dependent on the actual H concentration x at which the transformation occurs. As pointed out by Weatherly [34], H must diffuse to form the hydride; hence it is debatable whether H builds up to the correct concentration ahead of, behind, or at the moving interface separating the hydride and matrix. Recent nanobeam electron diffraction experiments performed by Barrow et al. [35] at room temperature have reported gradients in H concentration at the hydride–matrix interface of δ-hydrides, from $x \sim 1$ to $x \sim 1.7$ over a distance of ~7 nm. Hence, those authors propose that precipitation at the matrix–hydride interface takes place with the metastable γ phase ($x \sim 1$) acting as a precursor to the equilibrium δ-hydride. The assumption that hydride precipitation takes place at $x \sim 1$ results in experimentally estimated values of $\Delta W = (390 \pm 100)$ J/mol and $e^T_{33} \approx 0.124$, which compares very well with a theoretical value $e^T_{33} \approx 0.121$ obtained using Eq. (5) and the (γ) transformation strain given by Eq. (7). Such quantitative agreement supports the idea that precipitation of δ hydride could occur through a martensitic-type transformation that involves a precursor γ phase.In this picture, while H is in solution it dilates the Zr lattice via a purely dilatational strain, represented essentially by the e^H_{ij} tensor measured by MacEwen et al. [23], or almost equivalently by the e^{hyd}_{ij} transformation strains proposed by Carpenter [20], given in Eq. (6). In this case the volume occupied by the protons is distributed anisotropically, but with a rather low degree of anisotropy $e^H_{33} - e^H_{11} \approx 0.02$. For a fixed H concentration, hydride precipitation involves a small change in volume but a qualitative change in the way this additional volume is accommodated by the metal lattice. After the invariant plane transformation of the Zr atoms, the extra volume associated with the protons is distributed much more anisotropically, via the transformation strains proposed by Weatherly [34], with $e^{hyd}_{33} - e^{hyd}_{11} \approx 0.17$.

Several conclusions can be drawn by adopting an invariant plane strain transformation. Firstly, we see that a uniaxial load applied normal to the c-axis of a grain would result in a smaller, opposite change in precipitation temperature, which may be difficult to be observed experimentally. Hence, little ΔT change is expected in Zr2.5%Nb pressure tubes and Zircaloy tubing for loads applied along the axial direction, because in both cases the c-axes of the crystals lie mainly on the radial-transverse plane. This makes an axial stress rather ineffective as a mean to modify the precipitation probability among different grains, explaining why hydride reorientation is not observed when loads are applied along the tubes axial direction [36].

4.5. Hydride nucleation and reorientation

Fig. 1c reveals that *partial* reorientation of the macroscopic hydride platelets occurred due to application of the load, in agreement with the results reported by Hardie and Shanahan [36] in their thorough study of hydride reorientation in Zr2.5%Nb. The observed microstructures can be discussed in terms of the results found in the present experiments, and the mechanisms previously proposed to explain hydride reorientation in Zr alloys. Dislocations are preferential nucleation sites because they produce a local increase in H concentration, and because they help to accommodate the strain mismatch resulting from hydride precipitation. For the martensitic mechanism proposed by Weatherly, there is an additional advantage for specific dislocation structures that could provide the transformation strains required for hydride formation, i.e., those given by Eq. (7). This is because partial dislocations of type $(\frac{1}{3}[1\,\bar{2}\,1\,0]$ can provide part of the shuffle required to transform the *hcp* Zr lattice into the *fcc* Zr sub-lattice. Hence, the circumferential hydrides observed in Fig. 1c (left) are

thought to be associated with the spatial inhomogeneity (of dislocations) left by the manufacturing process, due to the intrinsic anisotropy of metal flow, as proposed by Marshall in his early investigations of this topic [37]. Marshall showed that the degree of hydride orientation observed in tubing can be described in terms of a *directional strain parameter* (DεP), characteristic of the actual manufacturing process, which quantifies the difference between the deformations introduced along each principal axes. At higher magnification, the macroscopic hydride platelets observed in Fig. 1c are in fact clusters of smaller sword-like hydrides, as explained Perovic et al. [8]. They proposed that such clusters form by a catalytic nucleation process, where the stress field of the first nucleus helps the nucleation of a second, smaller, nucleus at a certain distance along a given direction of the crystal. The cluster is formed by repetition of this process until the stress produced in the matrix by the last nucleus is not enough to override the activation barrier for the next nucleus at nearby potential sites. The formation of such cluster is fast, only limited by the availability of H, or intersection with grain boundaries. The orientation of this cluster or *array* is dictated by the location of the *next* preferential site on the array, which depends on the precise stress state in the neighborhood of a freshly created nucleus. The actual stress tensor results from contributions on different length scales. These include microscopic (Type 3) stresses from previous precipitates and existing dislocations, intergranular (Type 2) stresses due to elastic or plastic incompatibility between α-Zr grains, and (Type 1) macroscopic residual stresses or external loads. As we have found here, the resulting interaction energy terms could offset the positive contributions of the misfit strain energy term in the activation energy ΔG^a by an amount that could be calculated from Eqs. (5) and (7), increasing the precipitation temperature at selected sites where H will accumulate on cooling. Hence, on average, the circumferential hydrides observed in Fig. 1c (left) have nucleated at a temperature of ~270 °C, and are largely composed by a large fraction of hydrides precipitated in m_{Tilted} grains (with the substructure described in Fig. 11b of Ref. [16]), presumably because these grains have the most favorable dislocation networks and, to a less extent, internal stresses produced by plastic incompatibility between grains. Application of a 225 MPa external load along the hoop direction provides an offsetting stress, acting on all grain orientations which overrides such advantages, creating new preferential nucleation sites with higher precipitation temperatures than when precipitated in m_{Tilted} grains. Hence, the radial hydrides observed in Fig 1c (right) have precipitated at a temperature of ~280 °C, and are composed of a large fraction of hydrides precipitated in m_{Hoop} and m_{Tilted} grains (with a substructure corresponding to a mixture of Fig. 11d and e of Ref. [16]).

In an early theoretical analysis of this process, Ells [38] concluded that hydride reorientation occurs at the nucleation stage. In our previous work, we have found a diffraction signature of hydride reorientation [16]. This is because the orientation of a hydride cluster manifest itself through the hydride stress state, so δ(1 1 1) interplanar distances measured normal to the platelet are considerable larger (~2800$\mu\varepsilon$) than those measured within the plane of the platelet. Here, we have observed that for the L2 specimen reorientation is already manifested by the very first hydrides precipitated at ~280 °C under the applied load (refer to Fig. 6a of Ref. [16]). This provides additional data that confirms that hydride reorientation occurs at the nucleation stage.

5. Conclusions

In Zr2.5%Nb pressure tube material, hydride precipitation and dissolution presents distinctive differences between differently oriented grains. The following observations have been made from synchrotron X-ray diffraction experiments during thermal cycling of pressure tube material charged with hydrogen up to concentration of 130 wt ppm H:

- Hydride precipitation takes place mainly at grains of two ideal orientations: (i) m_{Hoop} grains, corresponding to crystallites having their *c*-axis along the tube hoop direction, the main texture component of the material, and (ii) m_{Tilted} grains, which have the *c*-axis pointing along an intermediate direction in the hoop–radial plane of the tube.
- On cooling from solid solution, hydride precipitation is more likely and occurs at a higher temperature (~5 °C) in m_{Tilted} grains than in m_{Hoop} grains.
- On heating from room temperature, dissolution of hydrides precipitated in m_{Hoop} grains occurs at lower temperatures (~15 °C) than those precipitated in m_{Tilted} grains.
- Application of a tensile load along the hoop direction during thermal cycling changes precipitation and dissolution temperatures, reducing the hysteresis in both grain families.
- Precipitation temperatures increase most for m_{Hoop} grains, at a rate of (0.08 ± 0.02) °C/MPa, in disagreement with previous theoretical estimations presented in the literature. At a load of 225 MPa the precipitation temperature in m_{Hoop} grains is larger or equal than in m_{Tilted} grains.
- The measured shift in precipitation temperature suggests that precipitation of δ hydride involves a martensitic transformation, where the volume increase associated to the protons is accommodated normal to the habit plane.
- The change in precipitation temperatures is accompanied by a large increase in the number of hydrides precipitated in m_{Hoop} grains. This redistribution of hydrides occurs on cooling, due to the observed changes in precipitation temperatures.
- Application of a load while H is in solution in the α-Zr matrix does not result in significant redistribution between different grain orientations.
- The connection between applied stress and change in precipitation temperature reported here should result in improved models to describe H redistribution during thermal cycling of Zr alloys.

Acknowledgments

The authors wish to thank A. Motta, K. Colas, M.R. Daymond and M. Kerr for experimental help and fruitful discussions; and the referees of this manuscript for many useful suggestions about interpretation of the present results. This research was partially funded by CONICET under PIP-542-2011, and by IAEA under Research Contract 17252. Usage of the Advanced Photon Source was supported by the U.S. Department of Energy, under Contract No. DE-AC02-06CH11357.

References

[1] Y. Fukai, The Metal–Hydrogen System: Basic Bulk Properties, Springer, 2005.
[2] M.P. Puls, Acta Metall. 32 (1984) 1259–1269.
[3] M.P. Puls, Acta Metall. 29 (1991) 1961–1968.
[4] W.H. Erickson, D. Hardie, J. Nucl. Mater. 13 (1964) 254–262.
[5] N. Paton, B. Hickman, D. Leslie, Metall. Mater. Trans. B 2 (1971) 2791–2796.
[6] H.K. Birnbaum, M.L. Grossbeck, M. Amano, J. Less Common Metals 49 (1976) 357.
[7] T.B. Flanagan, N.B. Mason, H.K. Birnbaum, Scripta Metall. 15 (1981) 109–112.
[8] V. Perovic, G.C. Weatherly, C.J. Simpson, Acta Metall. 31 (1983) 1381–1391.
[9] B.W. Leitch, M.P. Puls, Metall. Mater. Trans. A 3 (1992) 797–806.
[10] J. Lufrano, P. Sofronis, H.K. Birnbaum, J. Mech. Phys. Solids 44 (1996) 179–205.
[11] C.J. Simpson, C.E. Ells, J. Nucl. Mater. 52 (1974) 289–295.
[12] W. Pardee, N. Paton, Metall. Mater. Trans. A 11 (1980) 1391–1400.
[13] M.P. Puls, The Effect of Hydrogen and Hydrides on the Integrity of Zirconium Alloy Components: Delayed Hydride Cracking, Springer, 2012.

[14] G.A. McRae, C.E. Coleman, B.W. Leitch, J. Nucl. Mater. 396 (2010) 130–143.
[15] B.F. Kammenzind, B.M. Berquist, R. Bajaj, P.H. Kreyns, D.G. Franklin, in: 12th Intern. Symp. on Zirconium in Nuclear Industry, ASTM STP 1354, 2000, pp. 196–233.
[16] M.A. Vicente-Alvarez, J.R. Santisteban, P. Vizcaino, A.V. Flores, A.D. Banchik, J.D. Almer, Acta Mater. 60 (2012) 6892.
[17] D.R. Haeffner, J.D. Almer, U. Lienert, Mater. Sci. Eng. A 399 (2005) 120–127.
[18] R.A. Holt, S.A. Aldridge, J. Nucl. Mater. 135 (1985) 246–259.
[19] R.A. Holt, P. Zhao, J. Nucl. Mater. 335 (2004) 520–528.
[20] G.J.C. Carpenter, J. Nucl. Mater. 48 (1973) 264–266.
[21] J.P. Giroldi, P. Vizcaíno, A.V. Flores, A.D. Banchik, J. Alloys Compd. 474 (2009) 140–146.
[22] O. Zanellato, M. Preuss, J.Y. Buffiere, F. Ribeiro, A. Steuwer, J. Desquines, J. Andrieux, B. Krebs, J. Nucl. Mater. 420 (2012) 537–547.
[23] S. MacEwen, C.E. Coleman, C. Ells, J. Faber jr, Acta Metall. 33 (1985) 753–757.
[24] R.S. Daum, Y.S. Chu, A.T. Motta, J. Nucl. Mater. 392 (2009) 453–463.
[25] I.G. Ritchie, K. Sprungmann, Atomic Energy of Canada, Report 1983 AECL-7806.
[26] D. Khatamian, J.H. Root, J. Nucl. Mater. 372 (2008) 106.
[27] A. Hellouin de Menibus, T. Guilbert, Q. Auzoux, C. Toffolon, J.-C. Brachet, J.-L. Bechade, J. Nucl. Mater. 440 (2013) 169–177.
[28] M.A. Vicente-Alvarez, J.R. Santisteban, G. Domizzi, J.D. Almer, Acta Mater. 59 (2011) 2210–2220.
[29] R. Kirchheim, J.P. Hirth, Acta Metal. 35 (1987) 2899–2903.
[30] C.E. Coleman, J.F.R. Ambler, Scripta Metall. 17 (1983) 77–82.
[31] R.L. Eadie, C.E. Coleman, Scripta Metall. 23 (1989) 1865–1870.
[32] S.Q. Shi, Scripta Mater. 41 (1999) 1115–1121.
[33] E. Zuzek, J.P. Abriata, A. San Martin, Bull. Alloy Phase Diagr. 11 (1990) 385.
[34] G.C. Weatherly, Acta Metall. 29 (1981) 501–512.
[35] A.T.W. Barrow, A. Korinek, M.R. Daymond, J. Nucl. Mater. 432 (2013) 366–370.
[36] D. Hardie, M.W. Shanahan, J. Nucl. Mater. 55 (1975) 1–13.
[37] R.P. Marshall, J. Nucl. Mater. 24 (1967) 49–59.
[38] C.E. Ells, J. Nucl. Mater. 35 (1970) 306–315.